Distance Dependence of Long-Range Electron Transfer in Cytochrome c Derivatives Containing Covalently Attached Cobalt Cage Complexes

David W. Conrad,[†,§] Hui Zhang,[‡] David E. Stewart,[‡] and Robert A. Scott*[,‡]

Contribution from the Departments of Chemistry and Biochemistry and the Center for Metalloenzyme Studies and University Computing and Networking Services, University of Georgia, Athens, Georgia 30602, and Department of Chemistry, School of Chemical Sciences, University of Illinois, Urbana, Illinois 61801. *Received April 30, 1992*

Abstract: Seven horse heart cytochrome *c* derivatives each with a single Co(diAMsar) cage complex covalently attached by carbodiimide coupling to a specific surface carboxylate side chain have been synthesized. Tryptic peptide mapping combined with Edman degradation and FAB-MS sequencing has identified the attachment sites in the seven derivatives to involve residues D2, E4, E21, E61, E62, E66, and E104. Characterization of these derivatives by UV–visible spectroscopy, circular dichroism spectroscopy, and differential pulse voltammetry suggests that the protein tertiary structure has changed little upon attachment of the Co(diAMsar) probe. Flash photolysis experiments using $Ru(bpy)_3^{2+}$ as an excited-state reductant or oxidant allow the measurement of the rate constant for intramolecular electron transfer (k_{et}) from Co^{II}(diAMsar) to the Fe(III) of heme *c* in each derivative, resulting in values for k_{et} ranging from 1.0 to 3.2 s^{-1} (at 25.0 °C, pH 7.0). The time-averaged Co(diAMsar)–heme *c* edge-to-edge distances were estimated from solvated molecular dynamics simulations on structural models for the seven derivatives on the basis of crystal structure coordinates for horse heart cytochrome *c* and Co(diAMsar). These distances range from ~14 Å (in derivative E66) to ~20 Å (in derivative D2), which would predict a 200-fold range of rates assuming a simple exponential through-space distance dependence. The molecular dynamics trajectories were also used to calculate time-averaged dominant pathways for electron transfer[1,2] in each derivative, resulting in the prediction of a 2000-fold range of rates. The relationship between the experimental intramolecular electron-transfer rate constants and the Co(diAMsar) attachment site is discussed in light of these predictions.

A desire to understand on a molecular level the mechanism of long-range electron transfer between donors and acceptors in a biological matrix (e.g., in mitochondrial or photosynthetic electron-transport chains) has prompted a number of recent experimental studies.[3-9] This work focuses on determination of the factors that control the rate of electron transfer through a polypeptide medium between redox sites separated by fixed, known distances in the 10–25-Å range. Such factors as the thermodynamic driving force and the inherent kinetic reactivity of the redox sites (as measured by nuclear reorganization energies), which are defined simply by the nature of the donor and acceptor, have a readily predictable effect on electron-transfer rates.[5] In contrast, the dependence of these rates on factors related to the disposition of the redox sites within the biological matrix is less well understood. The donor–acceptor separation distance, the relative orientation of donor and acceptor, and the nature of the intervening medium all affect the overlap of acceptor and donor orbitals, controlling the magnitude of the electron tunneling matrix element, and thus the rate of electron transfer. Current emphasis in this field is on determining the distance dependence of the rate of long-range biological electron transfer and on investigating how the electronic structure of the intervening polypeptide medium might influence this rate. These factors may be involved in evolutionary control of the rate *and* specificity of physiological electron-transfer reactions.

With the simplistic assumption of a constant dielectric protein interior, the rate of intraprotein electron transfer is predicted to fall off exponentially with the through-space donor–acceptor (edge–edge) distance (d) in the nonadiabatic regime (eq 1).[5]

$$k_{et} = k_0 \exp[-\beta(d - d_0)] \quad (1)$$

There is some evidence for an approximately exponential distance dependence (with $\beta \approx 0.9$ Å^{-1}) of intramolecular heme–$(NH_3)_5$Ru–His electron-transfer rates in a series of "ruthenated" myoglobin and cytochrome *c* derivatives.[3] The work described herein involves the design of a set of cytochrome *c* derivatives with donor complexes covalently attached at different surface residues within which the distance dependence of the intramolecular electron-transfer rates has been measured.

Materials and Methods

The macrocyclic cage complex $Co(diAMsar)^{3+}$ was prepared according to the original synthesis given by Sargeson et al.[10] Tris(2,2′-bipyridine)ruthenium(II) chloride and 3-bromopropionic acid were purchased from Sigma. Nickel(II) hexamethyltetraazacyclodecane ($Ni^{II}Me_6$ane) was prepared according to literature procedures.[11,12] Horse heart cytochrome *c* (type VI) (Sigma) was purified to remove deamidated and polymeric forms by cation-exchange chromatography on CM52 cellulose (Whatman) as first described by Margoliash and co-workers.[13] The protein (75 mg/mL) was dissolved in 25 mM sodium phosphate buffer (pH 7) and the solution was oxidized by 1 molar equiv of $[Co(phen)_3](ClO_4)_3$ and loaded onto a column of the resin which had been previously equilibrated with 75 mM sodium phosphate buffer (pH 7). The protein was eluted isocratically at a flow rate of (10 mL/cm^2)/h.

Coupling Reaction. Two solutions were utilized for the coupling of $Co(diAMsar)^{3+}$ to cytochrome *c*. The first contained 150 mg of the purified protein in 9.0 mL of 75 mM sodium phosphate buffer (pH 7.0). The second one was prepared by dissolving 7.0 g of $[Co(diAMsar)H_2]Cl_5$ in 15 mL of water and adjusting the pH of the resulting solution to 4.75

* Author to whom correspondence should be addressed at the Department of Chemistry, University of Georgia.
† University of Illinois.
‡ University of Georgia.
§ Present address: Department of Chemistry, Illinois State University, Normal, IL 61761.

(1) Onuchic, J. N.; Beratan, D. N. *J. Chem. Phys.* **1990**, *92*, 722–733.
(2) Beratan, D. N.; Onuchic, J. N.; Betts, J. N.; Bowler, B. E.; Gray, H. B. *J. Am. Chem. Soc.* **1990**, *112*, 7915–7921.
(3) Therien, M. J.; Chang, J.; Raphael, A. L.; Bowler, B. E.; Gray, H. B. *Struct. Bonding* **1991**, *75*, 109–129.
(4) McLendon, G. *Acc. Chem. Res.* **1988**, *21*, 160–167.
(5) Marcus, R. A.; Sutin, N. *Biochim. Biophys. Acta* **1985**, *811*, 265–322.
(6) Millett, F.; Durham, B. In *Metal Ions in Biological Systems*; Sigel, H., Sigel, A., Eds.; Marcel Dekker: New York, 1991; Vol. 27, pp 223–264.
(7) Isied, S. S. In *Metal Ions in Biological Systems*; Sigel, H.; Sigel, A., Eds.; Marcel Dekker: New York, 1991; Vol. 27, pp 1–56.
(8) Sykes, A. G. *Struct. Bonding* **1991**, *75*, 1.
(9) Scott, R. A.; Conrad, D. W.; Eidsness, M. K.; Gorren, A. C.; Wallin, S. A. In *Metal Ions in Biological Systems*; Sigel, H., Sigel, A., Eds.; Marcel Dekker: New York, 1991; Vol. 27, pp 199–222.
(10) Geue, R. J.; Hambley, T. W.; Harrowfield, J. M.; Sargeson, A. M.; Snow, M. R. *J. Am. Chem. Soc.* **1984**, *106*, 5478–5488.
(11) Tait, A. M.; Busch, D. H. *Inorg. Synth.* **1978**, *18*, 2–9.
(12) Barefield, E. K.; Wagner, F.; Herlinger, A. W.; Dahl, A. R. *Inorg. Synth.* **1976**, *16*, 220–225.
(13) Brautigan, D. L.; Ferguson-Miller, S.; Tarr, G. E.; Margoliash, E. *J. Biol. Chem.* **1978**, *253*, 140–148.

0002-7863/92/1514-9909$03.00/0

by the dropwise addition of 5 M NaOH. The two solutions were then mixed and diluted with water to give a final volume of 30 mL. The pH was then readjusted to 4.75 by the dropwise addition of 1 M HCl. To this stirred reaction mixture was added 22 mg of 1-ethyl-3-(3-(dimethylamino)propyl)carbodiimide hydrochloride (EDC) (protein sequencing grade, Sigma). After 30 min, the reaction was terminated by separation of the reactants using gel filtration chromatography (Bio-Gel P-6 (Bio-Rad), 2.5 × 45 cm column previously equilibrated with 125 mM ammonium acetate buffer, pH 4.75). The red protein-containing band was collected and treated with 10 mg of $[Co(phen)_3](ClO_4)_3$ to fully oxidize any reduced protein formed during the coupling procedure.

Separation of Co(diAMsar)-cytochrome *c* Derivatives. The protein from the gel filtration column was then applied to a cation-exchange column (CM-52 cellulose, 2.6 × 33 cm) to isolate the cobalt-modified derivatives. Separation was achieved using a linear elution gradient between 1.0 L each of 125 and 650 mM ammonium acetate buffer (pH 7.0). Each of the Co(diAMsar)-labeled derivatives was rechromatographed using a Pharmacia/LKB FPLC system consisting of a GP-250 gradient programmer, two P-500 pumps, a UV-1 detector, and a Kipp & Zonen recorder. The initial separation employed a prepacked HR 5/5 Mono S column (Pharmacia) and a linear elution gradient between 0.35 M ammonium acetate, pH 8.0 (buffer A), and 1.35 M ammonium acetate, pH 6.0 (buffer B). The chromatograms were developed with gradients from 0% B to 60% B in 20 mL. The material which eluted was finally rechromatographed for a second time using the same HR 5/5 Mono S column and elution conditions.

Peptide Mapping. Protein samples (1 mg of protein/200 μL of 100 mM ammonium bicarbonate, pH 8.5) were digested by the addition of 3 μL of a fresh TPCK-treated trypsin solution (0.4 mg/mL in the above buffer solution). The samples were stirred for 3 h at 37 °C, after which a second 3-μL addition of trypsin was made and the digestion allowed to proceed for an additional 2 h. Samples were then lyophilized and stored at −20 °C. Reversed-phase peptide maps were constructed by dissolving 0.5 mg of protein digest in 250 μL of 0.1% aqueous trifluoroacetic acid (TFA) and injecting onto a HR 5/5 PepRPC column (Pharmacia). Separation was achieved using segmented elution gradients between 0.1% TFA (eluant A) and 0.1% TFA/20% water/80% acetonitrile (eluant B). Peptide samples were loaded and eluted with a gradient of 0% B to 0% B in 2 mL, followed by 0% B to 50% B in 35 mL. Material eluting in the void volume and individual peptide peaks were collected as fractions. Peptides unbound by the reversed-phase column were chromatographed on a HR 5/5 Mono S column using an elution gradient formed between 0.05 M ammonium acetate, pH 7.0 (buffer A), and 2 M ammonium acetate, pH 7.0 (buffer B). The chromatogram was developed with a linear gradient from 0% B to 50% B in 40 mL. All of the purified peptide fractions collected from RPC or cation-exchange chromatography were transferred to acid-cleaned vials, lyophilized, and stored at −20 °C until needed for further analysis.

Samples of lyophilized peptide fractions (10 μg) from RPC were dissolved in 0.1% aqueous TFA and submitted for low-resolution fast atom bombardment mass spectrometry (FAB-MS) using a ZAB-SE reverse-geometry ultrahigh-resolution spectrometer in the Magic Bullet matrix. For some peptides, further structure and sequence information was obtained by performing MS/MS on the parent ion peak using a 70-SE-4F spectrometer. Both spectrometers were operated by the staff of the Mass Spectrometry Laboratory at the University of Illinois.

Samples were also prepared for subsequent amino acid analysis by reacting approximately 150 μg of the given peptide in 1 mL of thoroughly deoxygenated 6 M HCl (Sequenal grade, Pierce). The hydrolysis reaction was allowed to proceed for 24 h at 110 °C. After cooling and lyophilization, the samples were redissolved in 130 μL of 200 mM sodium citrate buffer, pH 2.2 (Pierce), and submitted for amino acid analysis in the Basic Medical Sciences Department of the University of Illinois using a Beckman Model 119 CL amino acid analyzer. Samples were submitted for peptide sequencing in solution form, as recovered directly from the HR 5/5 PepRPC column, to the Biotechnology Center at the University of Illinois.

Physical Characterization. Absorbance spectra were obtained at room temperature using either a Cary 219 (Varian) or a Hewlett-Packard 8450A diode array spectrophotometer. Cobalt and iron analyses were performed on native and Co(diAMsar)-modified proteins (1 mg/mL in 100 mM sodium phosphate buffer, pH 7.0) by atomic absorption spectrometry using a Model 975 AtomComp inductively-coupled argon plasma spectrometer (Jarrell-Ash) at the Illinois Natural History Survey laboratory. The heme iron was also determined spectrophotometrically using published extinction coefficient values.[14] Circular dichroism (CD) spectra were obtained at 25 °C in 1-cm cylindrical quartz cells using a Jasco J500 C spectropolarimeter equipped with a DP-50 IN data station in the laboratory of M. K. Johnson at the University of Georgia.

All electrochemical measurements were made using either a cybernetic potentiostat prototype of the BAS-100A electrochemical analyzer (Bioanalytical Systems) or the commercial instrument itself. Edge-plane pyrolytic graphite (EPPG) electrodes were employed for the unmediated electrochemistry at scan rates of 20 mV/s (cyclic voltammetry) or 4 mV/s (differential pulse voltammetry) using 20 mM sodium phosphate/100 mM sodium perchlorate, pH 7.0, as the supporting electrolyte. Potentials were measured versus a Ag/AgCl reference electrode. Samples were purged of oxygen by solvent-saturated argon, and an argon atmosphere was maintained over the solution during measurements. Data were plotted using either a HIPLOT or a DMP-40 Series digital plotter (Houston Instruments). All experiments were performed at room temperature.

Flash Photolysis. Conventional flash photolysis experiments were performed using an apparatus[15] consisting of two linear FX-142C-4.5 xenon flash lamps (EG&G) connected in series and mounted parallel to a cylindrical sample cell. The flash lamp power supply, used to charge a bank of three 2-μF capacitors, contained a high-voltage power supply (20 kV) regulated by a Variac. A GP-86 triggered spark gap (EG&G) was used as a holdoff switch to isolate the high voltage from the flash lamps until firing was initiated. The lamps were flashed by applying a pulse from a Model T1700 high-voltage trigger transformer (EG&G) to the spark gap which allowed it to conduct and discharge the capacitor bank into the lamps. The spark gap switch had a useful operating range of between 6 and 16 kV, and typical experiments employed flashes at 6–8 kV (150–400 J/flash, $\tau_{1/2} \sim 80$ μs). The monitoring beam was the dc output of a tungsten-filament quartz halogen projector lamp (100 W) installed in an Illumination Industries LH-353Q lamphousing and powered by a Model 1152/1144 universal power supply (Schoeffel Instruments Corp.). The beam was shuttered using a Uniblitz electronic shutter controlled by a Model 100-2B shutter drive unit (A. W. Vincent Associates, Inc.). Excitation filtering was achieved using a Corning 3-69 color filter (513–527 nm, long-pass). The beam was focused on the sample cell by a UV grade fused silica lens (*f*/18). After passing through the sample cell, it was refocused using a UV grade fused silica lens (*f*/5) onto the entrance slit of a Model H20 monochromator (Instruments, SA, Inc.). Detection was accomplished with a R928 photomultiplier tube (PMT) (Hamamatsu), operated at 750 V and 5 °C, using a Model HTV C448A regulated dc power supply (Hamamatsu). A photodetector was located inside the photolysis enclosure to trigger data acquisition. It consisted of a MRD300 phototransistor (Motorola) powered by a 9-V battery. Upon firing of the lamps, the phototransistor sent a voltage pulse (4-μs rise time) to the external trigger input of a Model 3091 digital storage oscilloscope (Nicolet) to start data collection. The data were transferred from the oscilloscope to a floppy disk on an interfaced IBM PC as every tenth data point, for a total of 400 points, by converting the data into pure ASCII character files. Data analysis was done using KFIT, a nonlinear least-squares-fitting program written by On-Line Instruments Systems, Inc.

Intramolecular electron transfer within each Co(diAMsar)-cytochrome *c* derivative was initiated by flash photolytic excitation of $Ru(bpy)_3^{2+}$. In "photoreductive" experiments,[16] Co^{III}(diAMsar)-cytochrome c^{3+} was used and the $Ru(bpy)_3^{2+*}$ excited state was used as a powerful reductant[17] to produce Co^{II}(diAMsar)-cytochrome c^{3+} which decayed spontaneously to Co^{III}(diAMsar)-cytochrome c^{2+}, which was monitored spectrophotometrically at 550 nm. EDTA was used as a reductive scavenger of $Ru(bpy)_3^{3+}$.[18] In "photooxidative" experiments,[19] Co^{II}(diAMsar)-cytochrome c^{2+} was used and the $Ru(bpy)_3^{2+*}$ excited state was used as a powerful oxidant[17] to produce Co^{II}(diAMsar)-cytochrome c^{3+} which again decayed spontaneously to Co^{III}(diAMsar)-cytochrome c^{2+}. The combination of nickel(II) hexamethyltetraazacyclodecane and 3-bromopropionic acid served as an effective oxidative scavenger of $Ru(bpy)_3^{+}$.[20]

Computational Methods. Molecular mechanics and dynamics simulations (using AMBER v3.0A and v4.0[21]) were used to estimate through-space distances and potential electron-transfer pathways[1,2] in the

(14) Margoliash, E.; Frohwirt, N. *Biochem. J.* **1959**, *71*, 570–572.

(15) Sullivan, R. J. Ph.D. Thesis, University of Illinois at Urbana-Champaign, 1990.

(16) Nocera, D. G.; Winkler, J. R.; Yocom, K. M.; Bordignon, E.; Gray, H. B. *J. Am. Chem. Soc.* **1984**, *106*, 5145–5150.

(17) Whitten, D. G. *Acc. Chem. Res.* **1980**, *13*, 83–90.

(18) Keller, P.; Moradpour, A.; Amovyal, E.; Kagan, H. *Nouv. J. Chim.* **1980**, *4*, 377–384.

(19) Lieber, C. M.; Karas, J. L.; Gray, H. B. *J. Am. Chem. Soc.* **1987**, *109*, 3778–3779.

(20) Becker, J. Y.; Kerr, J. B.; Pletcher, D.; Rosas, R. *J. Electroanal. Chem. Interfacial Electrochem.* **1981**, *117*, 87–99.

(21) Pearlman, D. A.; Case, D. A.; Caldwell, J. C.; Seibel, G. L.; Singh, U. C.; Weiner, P.; Kollman, P. A. AMBER 4.0. University of California, San Francisco, 1991.

Table I. Identification of Co(diAMsar) Attachment Sites in Modified Tryptic Fragments

fraction[a]	tryptic fragment[b]	MH^+ m/z exptl (calc)[c]	sequence[d]
F_1	T18 (101–104)	787 (787)	Ala-Thr-Asn-(^{104}*Glu*)
F_2	T4 (14–22)H	1987 (1987)	(Cys)-Ala-Gln-(Cys)-His-Thr-Val-(^{21}*Glu*)-Lys
G_1	T11 (61–72)	1848 (1848)	Glu-(^{62}*Glu*)-Thr-Leu-Met-Glu-Tyr-Leu-Glu-Asn-Pro-Lys
G_2	T11 (61–72)	1848 (1848)	(^{61}*Glu*)-Glu-Thr-Leu-Met-Glu-Tyr-Leu-Glu-Asn-Pro-Lys
H_1	T1 (1–5)	942 (942)	Ac-Gly-Asp-Val-(^{4}*Glu*)-Lys[e]
H_2	T1 (1–5)	942 (942)	Ac-Gly-(^{2}*Asp*)-Val-Glu-Lys[e]
I	T11 (61–72)	1848 (1848)	Glu-Glu-Thr-Leu-Met-(^{66}*Glu*)-Tyr-Leu-Glu-Asn-Pro-Lys

[a] Fraction from FPLC Mono-S rechromatography (Figure 1). [b] Modified tryptic fragment from reversed-phase peptide map and corresponding region of sequence (H indicates heme-containing peptide). [c] Mass/charge ratio of parent ion of peptide fragment in FAB-MS. Calculated mass is given in parentheses. [d] Sequence determined by Edman degradation. Residues in parentheses were not identified (in T4 the two Cys residues covalently attach the heme *c*), and italic residues are the derived Co(diAMsar) attachment sites. [e] Sequences for modified T1 fragments deduced from MS/MS fragmentation patterns (e.g., see Table II).

Co(diAMsar)-cytochrome *c* derivatives. Crystallographic coordinates for horse heart cytochrome *c* were generously provided by Dr. Gary Brayer[22] and were used for all molecular mechanics and dynamics simulations. Coordinates for Co(diAMsar) were modeled upon the crystallographic coordinates for Co(sepulchrate)$(NO_3)_3$.[23] Co(diAMsar)-Glu and -Asp residues were constructed and mutated into the appropriate sequence positions using the Sybyl molecular modeling package (Tripos Associates, St. Louis). The force field used for the molecular mechanics and dynamics simulations was the standard AMBER force field,[24] with parameters for heme *c* adapted from Lopez and Kollman.[25] Force-field parameters for Co(diAMsar) were obtained from the literature.[26] For 110-ps molecular dynamics simulations (vide infra), a 6-Å-thick shell of ca. 760 TIP3A water molecules was included. In the 510-ps simulation, a 42 × 39 × 32 Å box of 919 TIP3A water molecules was included, periodic boundary conditions were used, and the simulation was run under constant-volume conditions. A constant dielectric of $\epsilon = 1$ and a nonbonded cutoff of 9.5 Å were used in all molecular dynamics simulations. Each solvated Co(diAMsar)-cytochrome *c* model was minimized for 3500 cycles. Time intervals of 0.002 ps were used for the molecular dynamics simulation, and the SHAKE algorithm was used to fix all the bond lengths throughout the simulation. Starting at 0 K, each minimized structure was heated to 300 K in 30 K increments applied every 0.2 ps. The subsequent equilibration process involved rerandomization of the velocity of each atom (corresponding to a Boltzmann distribution at 300 K) every 100 steps for a period of 2 ps, followed by a 6-ps period of stabilization. Following the heating and equilibration, data collection continued for at least 100 ps with coordinates saved every 1 ps for analysis. The molecular dynamics simulations were performed either on a Cyber 205 (~30 CPU hours for a 110-ps simulation involving 3400 atoms) or on a cluster of ten IBM Risc System/6000-550 computers (~60 CPU hours for a 110-ps simulation involving 3850 atoms), both supported by the University of Georgia Computing and Networking Services.

The Pathways (v2.1) algorithm developed by Beratan and co-workers[1] was provided by David Beratan and was used to identify possible electron-transfer pathways and calculate the "through-bonds" electronic coupling for each. When pathway searches were performed on cytochrome *c* structures without the Co(diAMsar) attached, atom OE1 of the modified residue's carboxylate was used as the donor atom; otherwise the Co atom was used. As an acceptor, the heme was "hardwired" so that pathway connections to any porphyrin ring carbon, His-18 imidazole ring atom, or Met-80 sulfur were all equally weighted. Only the dominant pathway's electronic tunneling matrix element ($\prod\epsilon$, the product of overlap decay factors for each pathway segment[2]) was considered for each structure, and $(\prod\epsilon)^2$ was used as a relative measure of the predicted rate of electron transfer. In the molecular dynamics simulations, a time-averaged electronic tunneling matrix element ($\langle(\prod\epsilon)^2\rangle$) was calculated and used as a relative measure of the electron-transfer rate.

Results

The several Co(diAMsar)-cytochrome *c* derivatives generated by the EDC-mediated coupling reaction described in Materials and Methods were identified and separated by cation-exchange chromatography (Figure 1), taking advantage of the increased positive charge (+4 units) of the derivatives compared to the unmodified protein. Atomic absorption spectroscopic determination of Fe and Co contents allowed preliminary identification of the nine peaks in Figure 1a. Peak A (50% of the total protein) is unmodified cytochrome *c*, peaks B–E (collectively 29% of the total protein) consist of Co-free carboxylate-modified cytochromes *c*, presumably containing *N*-acylurea EDC-modified glutamic or aspartic acid residues, and peaks F–I all display Co:Fe ratios of 1:1 (±5%). Rechromatography of peaks F–I (individually) on an FPLC Mono-S column yielded purification of seven Co(diAMsar)-cytochrome *c* derivatives (Figure 1b–e).

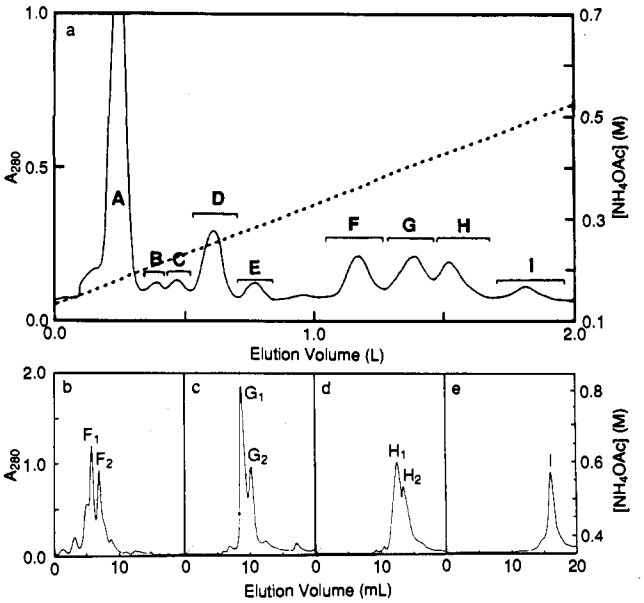

Figure 1. Cation-exchange elution profile for the Co(diAMsar)-cytochrome *c* coupling reaction product mixture. (a) Separation of crude reaction mixture on a 2.6 × 33 cm CM-52 column using 1 L of 0.125 M NH_4OAc, pH 7.0 (buffer A), and 0.650 M NH_4OAc, pH 7.0 (buffer B). Individual Co(diAMsar)-cytochrome *c* derivatives (fractions F–I) were rechromatographed on an FPLC HR 5/5 Mono S column as shown in (b)–(e). For these separations, buffer A was 0.35 M NH_4OAc, pH 8.0, buffer B was 1.35 M NH_4OAc, pH 6.0, and a linear gradient from 0% B to 60% B in 20 mL at 1.5 mL min^{-1} was used. All gradients are shown as dashed lines.

Identification of the attachment site of Co(diAMsar) in each of these derivatives was accomplished by sequencing the modified fragments from reversed-phase tryptic peptide maps. Unique peptide fragments that appeared in these maps (e.g., Figure 2) or that appeared in cation-exchange elution profiles of the reversed-phase column void volume (see Materials and Methods) were collected and subjected to amino acid analysis, Edman degradation sequencing (except for tryptic fragment T1, which is blocked), and FAB-MS. The amino acid analysis provided definitive identification of the tryptic fragment, and FAB-MS revealed the Co(diAMsar) content of the fragment. Sequencing generally allowed identification of the residue to which Co(diAMsar) was attached since this residue did not elute at the known

(22) Bushnell, G. W.; Louie, G. V.; Brayer, G. D. *J. Mol. Biol.* **1990**, *214*, 585–595.
(23) Creaser, I. I.; Geue, R. J.; Harrowfield, J. M.; Herlt, A. J.; Sargeson, A. M.; Snow, M. R.; Springborg, J. *J. Am. Chem. Soc.* **1982**, *104*, 6016–6025.
(24) Weiner, S. J.; Kollman, P. A.; Nguyen, D. T.; Case, D. A. *J. Comput. Chem.* **1986**, *7*, 230–252.
(25) Lopez, M. A.; Kollman, P. A. *J. Am. Chem. Soc.* **1989**, *111*, 6212–6222.
(26) Comba, P. *Inorg. Chem.* **1989**, *28*, 426–431.

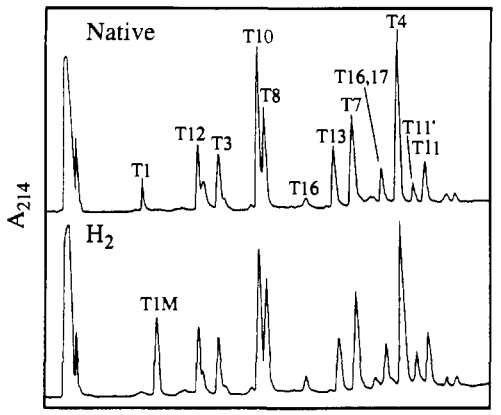

Figure 2. Reversed-phase HPLC elution (C_{18} column) of tryptic digests of native horse heart cytochrome *c* (top) and fraction H_2 from Figure 1d (bottom). Tryptic fragments of native horse heart cytochrome *c* are defined as follows ((*x*–*y*) is the peptide fragment consisting of residues *x*–*y*)[30]: T1, (1–5); T2, (6–7); T2′, (6–8); T3, (9–13); T4, (14–22)H; T5, (23–25); T6, (26–27); T7, (28–38); T7′, (28–39); T8, (40–53); T9, (54–55); T10, (56–60); T11, (61–72); T11′, (61–73); T12, (74–79); T12′, (73–79); T13, (80–86); T14, (87–88); T15, (89–91); T16, (92–97); T17, (98–99); T18, (101–104); T18′, (100–104). T16,17 is the concatenated peptide spanning T16 and T17 (92–99). The modified tryptic fragment T1M was identified by FAB-MS to be modified at D2 (see text).

Table II. Fragments and Molecular Ions Detected in MS/MS of the Modified T1 Tryptic Fragment from the Peptide Map of Fraction H_1

fragment	MH^+ *m/z* exptl (calc)
Ac-Gly-Asp-Val-[Glu-Co(diAMsar)]-Lys	942 (942)
Ac-Gly-Asp-Val-Glu-Co(diAMsar)	814 (814)
Ac-Gly-Asp-Val-Glu-Lys	588 (588)
Glu-Co(diAMsar)	484 (484)
Co(diAMsar)	371 (371)
Gly-Asp	171 (171)

position of any of the standard residues. This information is summarized in Table I. For the cases in which the modification site occurred in tryptic fragment T1, the modified peptide fragmentation pattern generated by MS/MS was used to identify the Co(diAMsar) attachment site. An example of such a fragmentation analysis for derivative H_1 is given in Table II.

The UV–visible spectra of all the Co(diAMsar)-cytochrome *c* derivatives appeared very similar to that for the native protein except for increased UV absorbance below ~300 nm.[9] Published extinction coefficients for native cytochrome *c* and for isolated Co(diAMsar) allowed the use of the UV region for an independent determination of Co(diAMsar):heme ratios of 1:1 (±10%) for all seven derivatives. Circular dichroism spectroscopy revealed insignificant differences between native cytochrome *c* and all of the Co(diAMsar)-cytochrome *c* derivatives, especially in the 200–250-nm region, indicating little change in overall tertiary structure.[9] The reduction potentials of heme *c* and Co(diAMsar) in each of the seven derivatives were measured by both cyclic voltammetry (CV) and differential pulse voltammetry (DPV) at an edge–plane pyrolytic graphite (EPPG) electrode (see Materials and Methods). Reversible waves were observed for both sites by CV (data not shown), and a typical DPV scan (for fraction I, Figure 1e) is shown in Figure 3. Reduction potentials for both sites in all seven derivatives are summarized in Table III.

For each Co(diAMsar)-cytochrome *c* derivative, both photooxidative and photoreductive flash photolysis experiments yielded a single-exponential time course for an increase in A_{550} (Figure 4). The absence of this kinetic phase in control experiments using unlabeled native cytochrome *c* (Figure 4) allows its assignment to a slow Co(II) → heme Fe(III) electron-transfer reaction. Figure 5 shows that, for each derivative, the first-order rate constants for this slow phase are independent of the Co(diAMsar)-cytochrome *c* concentration. We therefore assign these rates to the intramolecular Co(II) → heme Fe(III) electron-transfer reactions,

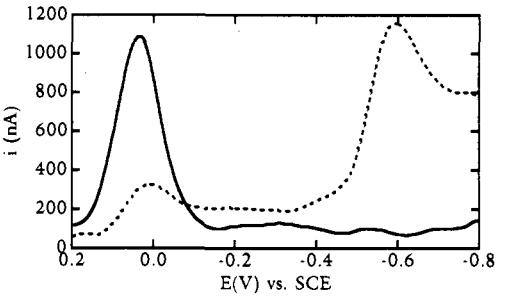

Figure 3. Differential pulse voltammograms for native cytochrome *c* (solid line) and Co(diAMsar)-cytochrome *c* derivative E66 (fraction I in Figure 1e) (dashed line) both recorded at an EPPG electrode at a scan rate of 4 mV s^{-1}, a pulse amplitude of 50 mV, and a pulse width of 50 ms. The samples were 0.5 mM protein in 20 mM sodium phosphate/100 mM sodium perchlorate, pH 7.0.

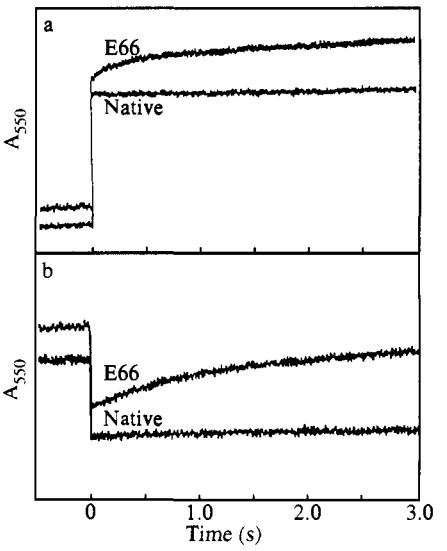

Figure 4. Spectrophotometric time progress curves after photoreductive (a) and photooxidative (b) flash photolysis (at $t = 0$) of native cytochrome *c* and the Co(diAMsar)-cytochrome *c* derivative E66. The slow increase of A_{550} present only for the E66 derivative in both (a) and (b) represents the intramolecular electron-transfer step. The sample in (a) consisted of 10 μM protein, 65 μM $Ru(bpy)_3^{2+}$, and 6.7 mM EDTA in 100 mM sodium phosphate, pH 7.0. The sample in (b) consisted of 10 μM protein, 65 μM $Ru(bpy)_3^{2+}$, 5 mM nickel(II) hexamethyltetraazacyclodecane, and 20 mM 3-bromopropionic acid in 100 mM sodium phosphate, pH 7.0.

Table III. Reduction Potentials of Co(diAMsar)-cytochrome *c* Derivatives Determined by Differential Pulse Voltammetry at an Edge–Plane Pyrolytic Graphite Electrode[a]

fraction	$E_{1/2}$(heme) (mV, NHE)	$E_{1/2}$(Co(diAMsar)) (mV, NHE)
F_1	269	−375
F_2	279	−369
G_1	264	−357
G_2	260	−361
H_1	264	−378
H_2	261	−374
I	261	−379

[a] Scan rate was 4 mV/s; pulse amplitude (ΔE) and width were −50 mV and 50 ms, respectively. All $E_{1/2}$ values were measured at 25 °C, are an average of five scans, and were calculated from $E_{peak} = E_{1/2} + \Delta E/2$. Errors in measurements are estimated as ±5 mV.

rate constants for which are summarized in Table IV. All seven rate constants are within a factor of 3 of one another.

Through-space distances between the Co^{II}(diAMsar) donor and the heme c^{3+} acceptor were estimated by molecular modeling techniques and are reported in Table V. The most meaningful distances are those between the nearest donor and acceptor atoms that are assumed to participate in the molecular orbitals involved

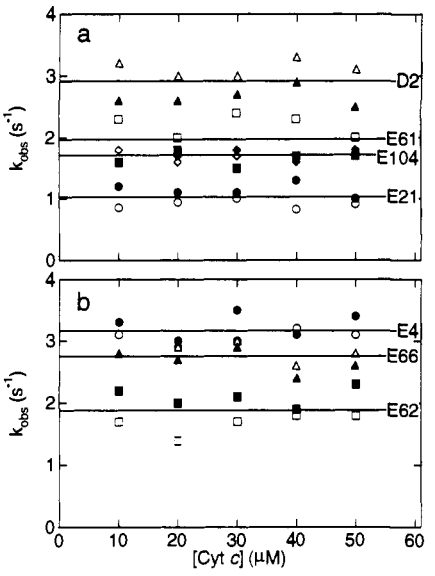

Figure 5. Protein concentration dependence of k_{obs} measured in both the photoreductive and photooxidative flash photolysis experiments for the seven Co(diAMsar)-cytochrome *c* derivatives. Open symbols refer to photoreduction and filled symbols refer to photooxidation experiments. The horizontal lines represent the weighted average of the k_{obs} values for all concentrations of the indicated derivatives. The experimental data are represented by the symbols. Top: ▲, D2; ■, E61; ◆, E104; ●, E21. Bottom: ●, E4; ▲, E66; ■, E62.

Table IV. Intramolecular Electron-Transfer Rate Constants of Co(diAMsar)-cytochrome *c* Derivatives Determined by Flash Photolysis with $Ru(bpy)_3^{2+}$

fraction[a]	derivative[b]	k_{et}^{red} (s^{-1})[c]	k_{et}^{ox} (s^{-1})[d]	$\langle k_{et} \rangle$ (s^{-1})[e]
F_1	E104	1.8 ± 0.1	1.7 ± 0.1	1.7 ± 0.1
F_2	E21	0.9 ± 0.1	1.2 ± 0.2	1.0 ± 0.2
G_1	E62	1.7 ± 0.2	2.1 ± 0.2	1.9 ± 0.3
G_2	E61	2.2 ± 0.2	1.7 ± 0.2	2.0 ± 0.3
H_1	E4	3.1 ± 0.1	3.3 ± 0.2	3.2 ± 0.2
H_2	D2	3.2 ± 0.2	2.6 ± 0.2	2.9 ± 0.3
I	E66	2.8 ± 0.1	2.7 ± 0.2	2.8 ± 0.2

[a] Chromatographic fraction from Figure 1b–e. [b] Attachment site from Table I. [c] Rate measured using $Ru(bpy)_3^{2+*}$ as a photoreductant. [d] Rate measured using $Ru(bpy)_3^{2+*}$ as a photooxidant. [e] Weighted average of k_{et}^{red} and k_{et}^{ox}.

in electron transfer. For the heme *c*, porphyrin ring carbons, His-18 imidazole ring atoms, and the Met-80 sulfur are considered as a group of acceptor atoms, and for Co(diAMsar), we used the six cage N ligand atoms as a group of donor atoms. In a preliminary account of this work,[9] the crystallographic coordinates of tuna cytochrome *c* (with appropriate residue replacements) were used to estimate distances from the heme *c* acceptor set to atom OE1 of the derivatized residue carboxylate, yielding the results in the first column of Table V. A similar exercise using the crystallographic coordinates of horse heart cytochrome *c*[22] yields the estimated distances in the second column of Table V. A better method of estimating such distances is using molecular dynamics to simulate the motions of the protein and Co(diAMsar) cage, followed by time averaging the appropriate distances. We have performed 110 ps of a molecular dynamics simulation on a solvated model of each of the Co(diAMsar)-cytochrome *c* derivatives, then searched each of the structures (generated every ps) during the 100 ps of data collection for the minimum distance between the donor and acceptor atom groups, and time averaged the resulting distances over the 100-ps time scale. This yields an average through-space distance and estimated standard deviation for each derivative (third column in Table V). For derivative E61, a longer (510-ps) molecular dynamics simulation was performed to ensure reasonable coverage of conformation space, especially for the Co(diAMsar) cage motion. The time-averaged distance over the 500 ps of data collection in that simulation is also given in Table V. This average distance is within experimental error of that calculated over the first 100 ps of the same trajectory, but the larger esd suggests that the other errors in the third column of Table V should probably be doubled, giving esd's of 1.0–1.5 Å. The time dependence of this minimum donor–acceptor through-space distance for derivative E61 over 500 ps of solvated molecular dynamics simulations is shown in Figure 6a. Figure 7 shows the dependence of the electron-transfer rate constants on through-space distance.

Table V. Heme–Co(diAMsar) Through-Space Edge–Edge Distances for Co(diAMsar)-cytochrome *c* Derivatives Calculated by Different Methods

	heme–Co(diAMsar) edge–edge distances (Å)		
derivative	tuna crystal structure[a]	horse crystal structure[a]	time-averaged MD simulation[b]
D2	19	18.7	19.8 ± 0.7
E4	17	19.2	18.9 ± 0.5
E21	10	13.8	18.2 ± 0.4
E61	14	16.0	16.3 ± 0.5
			16.8 ± 0.9[c]
E62	16	15.1	15.0 ± 0.4
E66	14	15.0	14.3 ± 0.7
E104	17	19.8	16.5 ± 0.7

[a] Measured as the distance from atom OE2 (Glu or Asp carboxylate O) of the modified residue to the nearest point on the heme (porphyrin ring C, His-18 ring atom, or Met-80 S). Numbers in first column (tuna crystal structure) are from ref 9. [b] Measured as the minimum distance between any ligand N atom of Co(diAMsar) and the nearest point on the heme. Measurements on structures at each picosecond of data collection in the 110-ps dynamic trajectory are averaged, yielding the esd's quoted. [c] Measured as in note *b*, with the time average done over 500 ps of data collection in the 510-ps dynamic trajectory of this derivative.

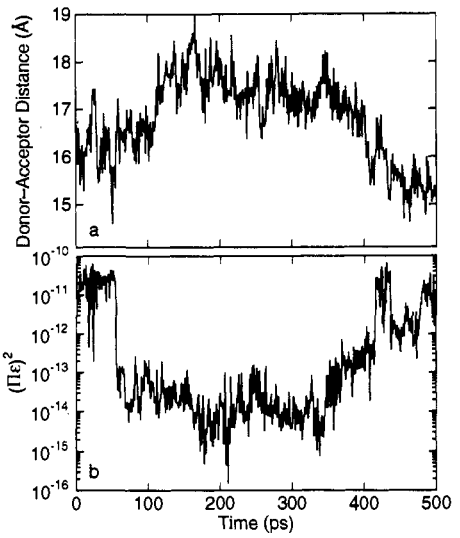

Figure 6. Computed time dependence of (a) the Co(diAMsar)–heme *c* edge-to-edge distance and (b) the square of the product of overlap decay factors for the dominant pathway, $(\Pi\epsilon)^2$, during 500 ps of data collection in a molecular dynamics simulation of the solvated Co(diAMsar)-cytochrome *c* E61 derivative. In (b), the highest values of $(\Pi\epsilon)^2$ (from 1 to 55 ps and from 416 and 436 ps) correspond to a pathway with the single "weak link" being an H-bond between the ε-NH of W59 and the carboxylate O of the heme propionate. All other pathways contain multiple H-bonds or through-space jumps.

Recent advances have been made in incorporating the nature of the intervening medium into theoretical predictions of electron-transfer rates.[1,2,27] Beratan, Gray, and co-workers have developed a simple method of estimating the electronic coupling of donor–acceptor wave functions through intervening polypeptide chains by segmenting potential electron-transfer "pathways" into sets of covalent bonds, H-bonds, and through-space gaps, each

(27) Jacobs, B. A.; Mauk, M. R.; Funk, W. D.; MacGillivray, R. T. A.; Mauk, A. G.; Gray, H. B. *J. Am. Chem. Soc.* **1991**, *113*, 4390–4394.

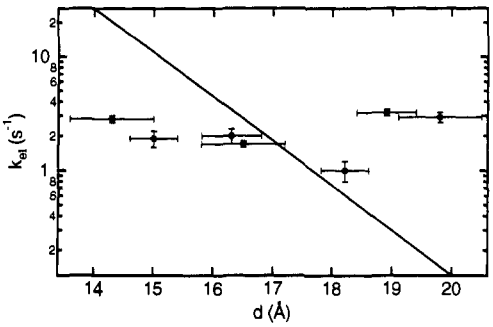

Figure 7. Distance dependence of k_{et} (●) for the seven Co(diAMsar)-cytochrome *c* derivatives. The solid line is calculated from eq 1 using $\beta = 0.9$ Å^{-1} and $d_0 = 3$ Å. The vertical error bars represent the estimated standard deviations in $\langle k_{et} \rangle$ from Table IV, and the horizontal error bars represent the estimated standard deviations in the 100-ps averaged edge-to-edge distances in the last column of Table V.

Table VI. Heme–Co(diAMsar) "Through-Bonds" Electronic Tunneling Matrix Elements for Co(diAMsar)-cytochrome *c* Derivatives

	relative tunneling matrix element		
		$\langle(\prod\epsilon)^2\rangle$	
derivative	$(\prod\epsilon)^2$ minimized[a]	without Co(diAMsar)[b]	with Co(diAMsar)[c]
D2	9.7×10^2	69	0.44
E4	6.8×10^2	1.3×10^2	2.9×10^{-2}
E21	9.1×10^5	4.5×10^5	59
E61	3.3×10^3	1.1×10^3	3.8 1.3[d]
E62	3.3×10^2	2.0×10^2	0.55
E66	4.1×10^4	3.9×10^3	8.6
E104	1.0	1.0	1.0

[a] Values calculated by Pathways v2.1[2] and normalized to the value for derivative E104 by dividing by 6.39×10^{-15}. [b] Values calculated for structures at each picosecond of data collection in a 110-ps dynamic trajectory of solvated unmodified horse heart cytochrome *c*, then averaged, and normalized to the value for derivative E104 by dividing by 1.12×10^{-12}. [c] Values calculated for structures at each picosecond of data collection in 110-ps dynamic trajectories of each solvated Co(diAMsar)-cytochrome *c*, then averaged, and normalized to the value for derivative E104 by dividing by 3.38×10^{-12}. [d] Calculated as in note *c*, but time averaged over 500 ps of the 510-ps dynamic trajectory.

of which contributes a defined decay factor to an overall electronic tunneling matrix element.[2] We have used this method (as implemented in the software package Pathways v2.1) to evaluate the electronic coupling between the Co(diAMsar) donor and heme *c* acceptor in each of our seven Co(diAMsar)-cytochrome *c* derivatives. The square of the product of the overlap decay factors, ϵ, for each segment of the dominant pathway yields a quantity that is directly proportional to the electron-transfer rate constant. These $(\prod\epsilon)^2$ quantities were extracted from a molecular mechanics energy-minimized model of each Co(diAMsar)-cytochrome *c* derivative and are listed in the first column of Table VI. The possibility that the nature of the dominant pathway and its derived tunneling matrix element may be time dependent suggested that a time-averaged $(\prod\epsilon)^2$ value over the time course of a molecular dynamics simulation might result in a more valid prediction of relative electron-transfer rates. The results of such an analysis for each attachment site derived from a 110-ps dynamic trajectory for unmodified cytochrome *c* are listed in the second column of Table VI, and the results based on seven 110-ps dynamic trajectories for the Co(diAMsar)-cytochrome *c* models are listed in the third column of Table VI. The time-averaged electronic tunneling matrix element for the 510-ps dynamic trajectory of derivative E61 is also included; its time dependence is shown in Figure 6b.

Discussion

The relatively slow intramolecular electron-transfer rates observed (~ 1 s^{-1}) are not unexpected, given the high reorganizational energy for the Co(II/III) redox in the cage complex (the difference in average Co–N bond lengths is 0.17 Å between the Co(II) and Co(III) oxidation states[23]). To compare these results with other similar rate constants in the literature, we can use the theoretical expression for k_{et} given in eqs 2 and 3.[5,28] In eq 2, $(H_{RP})^2$ is the

$$k_{et} = (4\pi^2/h)(H_{RP})^2(FC) \quad (2)$$

$$FC = (4\pi\lambda k_B T)^{-1/2} \exp[-(\lambda + \Delta G^\circ)^2/4\lambda k_B T] \quad (3)$$

square of the matrix element describing the electronic coupling between reactants (R) and products (P) and FC is the Franck–Condon factor describing the Boltzmann-weighted sum of overlaps of reactant and product vibrational levels, described in a classical sense by eq 3. In eq 3, λ is the reorganizational energy, ΔG° is the driving force, k_B is Boltzmann's constant, and T is the absolute temperature. Our systems employ ground-state electron transfer in cytochrome *c* and are expected to resemble the Ru(II) → Fe(III) electron-transfer reaction in the RuA_5 (His-33) (cytochrome *c*) derivative.[3] Using $\lambda = 1.2$ eV and $\Delta G^\circ = -0.18$ V,[3] we calculate that H_{RP} must be 0.024 cm^{-1} to predict the observed rate constant of 30 s^{-1}.[3] Assuming similar electronic couplings for our Co(diAMsar) derivatives ($H_{RP} = 0.024$ cm^{-1}), $\Delta G^\circ = 0.64$ V (Table III) and $\lambda = 2.1$ eV,[29] eq 2 predicts $k_{et} = 5.2$ s^{-1}, very close to the values that we measure. This electronic coupling is expected to fall off as the attachment site becomes more remote (for example in the D2 or E4 derivatives), giving rise to even slower rates, but this trend is not observed.

Hypothesizing an exponential distance dependence as described by eq 1 with $\beta = 0.9$ Å^{-1} would predict a $\sim$200-fold decrease in k_{et} from $\sim$14 to $\sim$20 Å (solid line in Figure 7), a trend that is clearly not seen in the measured rates (that span a range of $\sim$×3). Several possible explanations for this distance independence exist. The trivial explanation that we are actually measuring an intermolecular rather than an intramolecular process, involving the reduction of a heme Fe(III) on one molecule by a Co^{II}(diAMsar) attached to another molecule, is ruled out by the observed concentration independence of the rates (Figure 5).

Another possibility is that the measured rates reflect a rate-determining step prior to the electron transfer. For example, a conformational transition may be required to bring each derivative into a productive conformation, within which intramolecular electron transfer is fast. Such a conformational gate might involve a protein conformational change, but this seems unlikely since the new conformation would have to significantly enhance the tunneling matrix element for every derivative, even though each derivative presumably uses a unique electron-transfer pathway through the protein. The conformational gate could involve motion of the Co(diAMsar) probe about its attachment site, yielding a productive positioning of the probe about twice per second. Every derivative might have similar probe dynamics, but it would be surprising for every derivative to sample a productive conformation at the same rate.

Other (experimental) tests can be used to decide among some of the possible explanations mentioned above. For example, if the observed rates describe a rate-determining conformational gating process, then factors such as redox driving force that affect only the intramolecular electron-transfer rate should not change the observed rates (as long as the conformational gate is still slower). One way to alter the redox driving force is to construct an analogous set of Co(diAMsar) derivatives of metal-substituted cytochromes *c*. If a conformational gate involving Co(diAMsar) probe dynamics is involved, we should be able to change all the rates by altering solvent characteristics such as ionic strength. Similar ionic strength dependences of the rates for all seven derivatives would support this explanation.

Assuming that we are indeed directly measuring the intramolecular Co(II) → heme Fe(III) electron-transfer rates, they

(28) Bertrand, P. *Struct. Bonding* **1991**, *75*, 1–47.
(29) Conrad, D. W.; Scott, R. A. *J. Am. Chem. Soc.* **1989**, *111*, 3461–3463.
(30) IUPAC-IUB Commission on Biochemical Nomenclature. *J. Biol. Chem.* **1967**, *242*, 555–557.

may all be the same because the donor–acceptor distances are not significantly different. It is conceivable that the Co(diAMsar) probes in the E66 and E62 derivatives spend most of their time in a conformation with a significantly longer donor–acceptor distance, whereas the D2 and E4 derivatives exhibit probe conformational distributions that are equally distorted toward shorter distances. Such distorted conformational distributions might be induced by electrostatic interactions of Co(diAMsar) with cytochrome *c* charged surface residues. However, 500 ps of a solvated dynamics simulation does not predict such significant conformational distortions for the E61 derivative (Figure 6a) and it would be very coincidental for all seven derivatives to occupy conformational distributions with about the same average probe–heme distances.

A more intriguing possible explanation is that the distances quoted in Table V are correct but that these *through-space* distances do not control the electron-transfer rates. In other words, perhaps the overlap of acceptor and donor orbitals (which should control the electron tunneling matrix element) is not simply predicted by long-range overlap of Gaussian tails of orbitals originating on Co(diAMsar) and heme *c* but is complicated by the presence of energetically accessible orbitals on intervening polypeptide chains. This would effectively constitute a *through-bonds* contribution to donor–acceptor electron transfer and if the through-bonds "pathways" for electron-transfer yield similar donor–acceptor wave function overlaps for all seven Co(diAMsar)-cytochrome *c* derivatives, the rates would be expected to be similar.

We have chosen to use the Pathways program developed by Beratan, Gray, and co-workers[1,2] as an initial test of the validity of this concept in explaining our rate constants. Using the product of overlap decay factors, ϵ, for the dominant pathway connecting donor and acceptor as a measure of the tunneling matrix element allows an estimation of the relative rate constants that are proportional to $(\prod\epsilon)^2$.[2] Using static energy-minimized structures of Co(diAMsar)-horse heart cytochrome *c* predicts rate constants that span a range of nearly 10^6 (first column of Table VI). A slightly smaller range is observed using time-averaged overlaps from a 110-ps molecular dynamics trajectory calculated on unmodified horse heart cytochrome *c* (second column of Table VI). However, when each Co(diAMsar)-modified structure is modeled individually, the time-averaged overlaps predict rate constants that span a much smaller range ($\sim 2 \times 10^3$; third column of Table VI). It is also noteworthy that the absolute values of $(\prod\epsilon)^2$ generally increase when they are time averaged to account for protein dynamics (e.g., the $(\prod\epsilon)^2$ for derivative E104 increases by over 2 orders of magnitude from the first to the second column of Table VI). Apparently, the flexibility of the protein allows for sampling of conformations that offer high-overlap pathways that dominate the time average (Figure 6b).

Neither the simple through-space distance-dependent model (Figure 7) nor the through-bonds "pathway" model (even using our most sophisticated solvated molecular dynamics time averaging as in the third column of Table VI) is successful in predicting the observed electron-transfer rate constants. It is unknown whether this represents a failure in the molecular modeling force field or in the theoretical electron-transfer models.

Conclusion

Co^{II}(diAMsar) attached to carboxylic acid side chains of a series of surface residues of horse heart cytochrome *c* transfers electrons by an intramolecular process to Fe(III) of the heme *c* prosthetic group. The rate of this electron-transfer reaction is nearly independent of the site of attachment of Co(diAMsar). Although several explanations for this result are possible, this study clearly demonstrates the need for more data before either the exponential through-space distance dependence or the through-bonds "pathway" model of long-range biological electron transfer can be generally accepted.

Acknowledgment. D.W.C. acknowledges Dr. Larry Faulkner for help and support in the final stages of this work. The authors thank Dr. Gary Brayer for providing horse heart cytochrome *c* coordinates and Dr. David Beratan for providing the Silicon Graphics IRIX version of the Pathways v2.1 program. University of Georgia Computing and Networking Services provided CPU time on the University Cyber 205 and IBM RS/6000-550 cluster for the molecular modeling calculations. This work was partially supported by an NSF Presidential Young Investigator Award (CHE 87-15889) to R.A.S. and an NSF Research Training Group Award (DIR 90-14281) to the Center for Metalloenzyme Studies, University of Georgia.